A unified description of the DC conductivity of monolayer and bilayer graphene based on resonant scatterers

A. Ferreira [1], J. Viana-Gomes[1], Johan Nilsson[2], N. M. R. Peres[1], and A. H. Castro Neto[3]
[1] *Department of Physics and Center of Physics, University of Minho, P-4710-057, Braga, Portugal*
[2] *Department of Physics, University of Gothenburg, 412 96 Gothenburg, Sweden and*
[3] *Department of Physics, Boston University, 590 Commonwealth Avenue, Boston, Massachusetts 02215, USA*
(Dated: June 28, 2010)

We show that a coherent picture for the DC conductivity of monolayer and bilayer graphene emerges from considering that strong short-range potentials are the main source of scattering in these two systems. The origin of the strong short range potentials may lie in adsorbed hydrocarbons at the surface of graphene. The equivalence between results based on the partial wave description of scattering and the $T-$matrix approach is established. The scattering formalism for electrons in a biased bilayer graphene is developed and the DC conductivity of that system is studied.

PACS numbers: 81.05.ue,72.80.Vp,78.67.Wj

I. INTRODUCTION

In is famous book,[?] Peierls noted that in three dimensions the first Born approximation cannot be used to deal with short range potentials in general, even when the potential is not too strong. The reason lies on the fact that the first Born approximation overestimates the value of the scattering cross section, and modifies the dependence of this latter quantity on the energy of the incoming particle relatively to the exact result.

In nuclear physics, two-dimensional scattering problems are irrelevant, and therefore Peierls did not discuss the validity of the first Born approximation in systems of reduced dimensions. As we can easily imagine, things can only *get worse*, because of the asymptotic logarithmic behavior of some of the Bessel functions, for small values of their arguments, which play an important role in low-energy scattering.

Contrary to nuclear physics, some condensed matter systems impose dimensional constraints on the electronic motion. Such constraints are a directly consequence of the lattice structure of the given solid. Electrons moving in graphene[? ? ?] face the most dramatic dimensional constraint, by being forced to move along a two-dimensional plane, formed by the honeycomb lattice, defined by the carbon atoms. In bilayer graphene, the electrons are also confined to move in two-dimensions. Since this latter system is a stacking of two graphene sheets, the electrons may hop between the layers.

As well as in nuclear and particle physics, scattering cross sections in condensed matter physics are of ultimate importance for the interpretation of the DC transport in solids, specially in what concerns the effect of localized impurities. These can be either described by short range or long range potentials. Following Peirels,[?] the correct interpretation of the conductivity of a metal at low temperatures may require to describe electronic scattering by impurities beyond the first Born approximation. This is specially true if the impurities give rise to strong short-range potentials.

In systems such as monolayer and bilayer graphene, where the electronic density can be tuned between zero and $\sim 10^{12}$ cm^{-2}, computing the correct dependence of the cross section on the Fermi energy is a crucial ingredient for a meaningful interpretation of the data.

Since the early days of graphene physics,[? ?] it became clear that the conductivity of monolayer graphene can show slightly sub-linear dependence on electronic density, which can be varied by using a back-gate. Given that the electronic density is proportional to the back-gate potential, V_g, the conductivity curves of monolayer and bilayer graphene are usually plotted against V_g. On the other hand, the conductivity of bilayer graphene shows, consistently, a robust linear dependence on V_g.

Both monolayer and bilayer graphene-based devices use sheets of the material produced in exactly the same manner, by exfoliation of graphite. It is by now believed that the limiting sources of scattering in graphene are introduce via the fabrication process of the devices.

The sources of disorder in graphene can vary. They can be due to adsorbed atoms (for example hydrogen) or molecules (for example hydrocarbons), extended defects, such as folded regions (wrinkles), vacancies, and topological defects (such as of Stone-Wales type, specially at the edges[?]). The system has a certain amount of rippling (random strain),[? ?] so it is not a perfect planar lattice, and it has rough edges, which can exhibit scrolling.[?] Additionally, the electrostatic random potential at the surface of the silicon oxide substrate acts as an additional scattering source, originated from charged impurities.[? ? ? ?]

It is widely accepted that the electron-hole puddles[? ?] forming in the material at the neutrality or Dirac point are due to localized subsurface charged impurities. Whether charged impurities are the limiting source of scattering in doped graphene remains unclear. Indeed, combined with charged scatterers, the resonant scattering mechanism, due to adsorbed hydrocarbons,[?] is currently ascending as one of the dominant processes limiting the electronic mobility in graphene.[? ?] As we show in Sec. III A, adsorbed hydrocarbons can effectively act as strong short-range scatterers, which can be mimic by a model of vacancies[?] in the honeycomb lattice.

Since the sources of scattering are, most likely, introduced by the fabrication process, they must be the same for both monolayer and bilayer graphene. Therefore, a consistent theoretical description of the conductivity of graphene has to be

able to describe the experimental curves of both monolayer and bilayer graphene, at low temperatures, invoking the same source of scattering. In the sections ahead, we will show that such consistent theoretical description can be achieved by considering strong short-range potentials, whose origin may lie in adsorbed chemical species at the surface of the material. Instrumental to our description, is the critical analysis developed by Peierls:[?] the calculation of the exact scattering cross sections may be essential to a correct interpretation of the data.

Before studying the DC conductivity data for both monolayer and bilayer graphene, a task we defer to Sec. III, we first survey the scattering theory for electrons in monolayer and bilayer graphene in Sec. II. This first step is essential to make understandable the treatment of Sec. III. In the process, we will show that the calculation of the DC conductivity of both monolayer and bilayer graphene can be easily done using the intuitive approach to scattering given the partial-wave analysis.

II. PARTIAL WAVE ANALYSIS OF STRONG SHORT RANGE POTENTIALS

As we discussed in the introduction, the calculation of the DC conductivity of a metal requires the calculation of the transport cross section, as accurately as possible. A well established approach requires the computation of the phase-shifts induced in the scattered electron wave function by the scattering potential. If the phase-shifts are known exactly, so it is the cross section. Below we fix the notation and introduce the central quantities needed in this work, by giving a concise presentation of the phase-shift approach to scattering, in the context of graphene and its bilayer.[? ? ? ?] These results will later be used in Sec. III. The scattering theory for electrons in a biased graphene bilayer has not been, to our best knowledge, developed so far in the literature, and therefore it is presented in Sec IV.

Scattering theory states that the large-distance wave function of a particle in the presence of a scattering potential must have the form (in two-dimensions)

$$\psi(\boldsymbol{r}) \simeq e^{ik_i x} + f(\theta)\frac{e^{ik_f r}}{\sqrt{r}}\,, \tag{1}$$

where $\boldsymbol{k}_i = (k, 0)$ and $\boldsymbol{k}_f = k(\cos\theta, \sin\theta)$ are the momentum of the incoming and scattered waves, respectively; clearly, we have $k_i = k_f = k$. The scattering amplitude, $f(\theta)$, can be written in terms of the phase-shifts, δ_m, associated with the partial-wave expansion of the scattered wave function in the basis of angular momentum states. In Eq. (1), the first term represents the incoming particle, with the incoming momentum oriented along the $x-$axis, and the second one represents the cylindrical scattered wave function.

As it stands, Eq. (1) holds for the two-dimensional Schrödinger equation.[?] However, for both graphene and graphene bilayer, the large distance behavior of the wave function differs slight but significantly from Eq. (1).

A. Electronic scattering in graphene

For graphene, the motion of the electrons in the $\pi-$orbitals is, at low energies, described by the two-dimensional massless Dirac Hamiltonian, reading[?]

$$H_{\boldsymbol{K}} = v_F \boldsymbol{\sigma}\cdot\boldsymbol{p}\,, \tag{2}$$

where the Fermi velocity is defined as $v_F = 3ta_0/(2\hbar)$, with t the hopping integral between the p_z orbitals of two adjacent carbon atoms, and $a_0 \approx 1.4$ Å is the carbon-carbon distance in graphene (see Fig. 1). The vector $\boldsymbol{\sigma}$ is written in terms of the Pauli's matrices as $\boldsymbol{\sigma} = (\sigma_x, \sigma_y)$, and $\boldsymbol{p}$ is the momentum operator.

fig_01.png

FIG. 1. (color online) Lattice structure and Brillouin zone of monolayer graphene. **Left:** the hexagonal lattice of graphene, with the next nearest neighbor, $\boldsymbol{\delta}_i$, and the primitive, $\boldsymbol{a}_i$, vectors depicted. The area of the primitive cell is $A_c = 3\sqrt{3}a_0^2/2 \simeq 5.1$ Å^2, and $a_0 \simeq 1.4$ Å. **Right:** the Brillouin zone of graphene, with the Dirac points $\boldsymbol{K}$ and $\boldsymbol{K}'$ indicated. Close to these points, the dispersion of graphene is conical and the density of states is proportional to the absolute value of the energy.

The wave functions of the Hamiltonian (2) have, in cartesian coordinates, the explicit form

$$|\psi_\pm\rangle = \frac{1}{\sqrt{2A}}\begin{pmatrix} 1 \\ \pm e^{i\theta(\boldsymbol{k})}\end{pmatrix} e^{i\boldsymbol{k}\cdot\boldsymbol{r}}\,, \tag{3}$$

with $\theta(\boldsymbol{k}) = \arctan(k_y/k_x)$ and A the area of the system. The energy eigenvalues corresponding to the wave function (3) are $E = \pm v_F\hbar k$. From this latter result, follows the density of states per spin, $\rho(E) = 2|E|/(\pi\sqrt{3}t^2)$. The probability density current reads[?]

$$\boldsymbol{J} = v_F\langle\psi_\pm|(\sigma_x, \sigma_y)|\psi_\pm\rangle\,. \tag{4}$$

For the study of scattering, it is more convenient to cast Hamiltonian (2) in cylindrical coordinates, r and θ, as

$$H_{\boldsymbol{K}} = -iv_F\hbar\begin{bmatrix} 0 & L_- \\ L_+ & 0\end{bmatrix}\,, \tag{5}$$

where the operators $L_\pm = e^{\pm i\theta}(\partial_r \pm ir^{-1}\partial_\theta)$ act on the Bessel functions as rising/lowering operators, according to the following result

$$L_\pm[C_m(kr)e^{i\theta m}] = \mp kC_{m\pm1}(kr)e^{i\theta(m\pm1)}\,. \qquad (6)$$

In Eq. (6) the function $C_m(kr)$ stands for $J_m(kr)$ and $Y_m(kr)$, the regular and irregular Bessel functions, respectively, and for the Hankel functions $H_m^{(1)}$ and $H_m^{(2)}$. For the modified Bessel function $K_m(kr)$ we have

$$L_\pm[K_m(kr)e^{i\theta m}] = -kK_{m\pm1}(kr)e^{i\theta(m\pm1)}\,. \qquad (7)$$

In cylindrical coordinates, the radial probability density current reads

$$J_r = v_F\langle\psi_\pm|\sigma_r|\psi_\pm\rangle\,, \qquad (8)$$

where σ_r is defined as

$$\sigma_r = \begin{pmatrix} 0 & e^{-i\theta} \\ e^{i\theta} & 0 \end{pmatrix}. \qquad (9)$$

The tangential component of the probability density current reads $J_\theta = v_F\langle\psi_\pm|\sigma_\theta|\psi_\pm\rangle$, with $\sigma_\theta = \sigma_r\mathrm{diag}(i,-i)$, where $\mathrm{diag}(i,-i)$ represents a diagonal matrix. Let us now derive, for massless Dirac electrons in two dimensions, the equivalent of the asymptotic wave function (1). To that end, we note that a state having the form

$$|\psi_m\rangle = \frac{1}{\sqrt{2A}}\begin{bmatrix} J_m(kr)e^{i\theta m} \\ \pm iJ_{m+1}(kr)e^{i\theta(m+1)} \end{bmatrix}, \qquad (10)$$

is also an eigenstate of the Hamiltonian (5). We start by assuming that the asymptotic (large r) behavior of the wave function in the angular momentum channel m has the form (from here on, we consider only $E > 0$)

$$|\psi_m\rangle \simeq \frac{1}{\sqrt{2A}}\sqrt{\frac{2}{\pi kr}}\begin{bmatrix} \cos(kr-\lambda_m+\delta_m) \\ ie^{i\theta}\sin(kr-\lambda_m+\delta_m) \end{bmatrix} e^{i\delta_m}\,, \qquad (11)$$

an ansatz inspired in the fact that the Hamiltonian (2) is a set of two coupled first-order differential equations, and in the asymptotic behavior of Bessel functions for large r:[?]

$$J_m(x) = \sqrt{\frac{2}{\pi x}}\cos(x-\lambda_m)\,, \qquad (12)$$

$$Y_m(x) = \sqrt{\frac{2}{\pi x}}\sin(x-\lambda_m)\,, \qquad (13)$$

with $\lambda_m = m\pi/2 + \pi/4$. Using Eq. (11), we write the total wave function as an expansion in partial waves, reading

$$|\psi\rangle = \sum_{m=-\infty}^{\infty} i^m e^{i\theta m}|\psi_m\rangle\,. \qquad (14)$$

Exploiting of the relation

$$e^{ikr\cos\theta} = \sum_{m=-\infty}^{\infty} i^m e^{i\theta m}J_m(kr)\,, \qquad (15)$$

we obtain

$$|\psi\rangle \simeq \frac{1}{\sqrt{2A}}\begin{pmatrix} 1 \\ 1 \end{pmatrix}e^{ikx} + \frac{1}{\sqrt{2A}}\begin{pmatrix} 1 \\ e^{i\theta} \end{pmatrix}f(\theta)\frac{e^{ikr}}{\sqrt{r}}\,, \qquad (16)$$

with the scattering amplitude reading

$$f(\theta) = \sqrt{\frac{2i}{\pi k}}\sum_{m=-\infty}^{\infty} e^{i\theta m}e^{i\delta_m}\sin\delta_m\,. \qquad (17)$$

It is a simple exercice to show that the first term in Eq. (16) corresponds to a flux $J_x = v_F/A$ (and $J_y = 0$), whereas to the second term corresponds a radial flux $J_r = v_F|f(\theta)|^2/(rA)$ (and $J_\theta = 0$). Then, according to the usual definition of differential cross section, $\sigma(\theta)$, it follows that

$$\sigma(\theta) = |f(\theta)|^2\,. \qquad (18)$$

Before we turn to scattering in bilayer graphene, it will be useful, for latter use, to introduce some more additional asymptotic forms of the Bessel functions $J_m(x)$, $Y_m(x)$, and $K_m(x)$, in addition to those already given in Eqs. (12) and (13). For large x, we have[?]

$$K_m(x) = \sqrt{\frac{\pi}{2x}}e^{-x}\,. \qquad (19)$$

For $x \ll 1$, the asymptotic forms read[?]

$$J_m(x) = (x/2)^m\Gamma^{-1}(m+1)\,, \qquad (20)$$

$$Y_0(x) = 2\pi^{-1}\ln x\,, \qquad (21)$$

$$Y_m(x) = -\pi^{-1}\Gamma(m)(x/2)^{-m}\,, \quad m = 1,2,\ldots\,, \qquad (22)$$

and

$$K_0(x) = -\ln x\,, \qquad (23)$$

$$K_m(x) = 2^{-1}\Gamma(m)(x/2)^{-m}\,, \quad m = 1,2,\ldots\,, \qquad (24)$$

where $\Gamma(x)$ is the gamma function. We now consider scattering in bilayer graphene.

B. Electronic scattering in bilayer graphene

The graphene bilayer has four atoms per unit cell, with the two honeycomb sheets arranged according to Bernal stacking, as shown in Fig. 2. Two of the atoms belonging to each of the layers are on top of each other (the atoms A_1 and B_2, in Fig. 2), allowing for inter-layer hopping. Such process is represented by a hopping parameter $t_\perp \approx 0.5$ eV. The other two carbon atoms, those termed A_2 and B_1 in Fig. 2, are not coupled to the carbon atoms of the other layer, in accordance with the assumptions of the minimal model electronic motion in bilayer graphene.

The band structure of bilayer graphene has four bands, but the low energy physics ($|E| < t_\perp$) can be described by an effective model of only two,[?] where the atoms linked by $t_\perp$ are projected out, since they describe high-energy bands – the

dimmer of atoms A_1 and B_2, linked by $t_\perp$, form a two-level system, with energy levels $\pm t_\perp$. Additionally, the atoms in the two sheets can be made non-equivalent by applying an electric field perpendicular to the sheets, inducing in this way a gap in the spectrum (the electrostatic potential difference between the two layers is $2V$).[??]

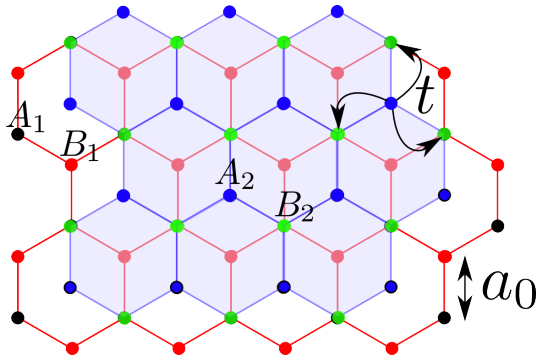

FIG. 2. (color online) Lattice structure of graphene bilayer. The atoms represented by the letters A_1 and B_1 lie on the bottom graphene layer, whereas the other two are in the top layer. The electrons can hop between layer via a perpendicular hopping parameter $t_\perp$ between the carbon atoms termed A_1 and B_2. The Brillouin zone of bilayer graphene is the same as that of monolayer graphene (see Fig. 1).

The derivation of the effective Hamiltonian is straightforward. We write the full Hamiltonian as

$$H = \begin{bmatrix} V & 0 & 0 & \hat{\pi} \\ 0 & -V & \hat{\pi}^\dagger & 0 \\ 0 & \hat{\pi} & -V & -t_\perp \\ \hat{\pi}^\dagger & 0 & -t_\perp & V \end{bmatrix} \equiv \begin{bmatrix} H_L & H_{LH} \\ H_{LH}^\dagger & H_H \end{bmatrix} , \quad (25)$$

where the columns of the Hamiltonian are labeled by the four atoms in the unit cell. In ascending order, this labeling is B_1, A_2, B_2, and A_1. The operator $\hat{\pi}^\dagger$ is defined as $\hat{\pi}^\dagger = -v_F\hbar(i\partial_x + \partial_y)$. The eigenproblem $H|\psi\rangle = E|\psi\rangle$ can be written as

$$\begin{bmatrix} H_L & H_{LH} \\ H_{LH}^\dagger & H_H \end{bmatrix} \begin{bmatrix} |\varphi\rangle \\ |\chi\rangle \end{bmatrix} = E \begin{bmatrix} |\varphi\rangle \\ |\chi\rangle \end{bmatrix} , \quad (26)$$

and the effective low-energy Hamiltonian we seek is that obeyed by the spinor $|\varphi\rangle$. It follows from Eq. (26) that

$$H_L|\varphi\rangle + H_{LH}(E - H_H)^{-1}H_{LH}^\dagger|\varphi\rangle = E|\varphi\rangle , \quad (27)$$

and considering that $t_\perp \gg (V, |E|)$, we have $H_{BL}|\varphi\rangle = E|\varphi\rangle$, with[?]

$$H_{BL} = V\sigma_z - \frac{V}{t_\perp^2}\begin{bmatrix} \hat{\pi}\hat{\pi}^\dagger & 0 \\ 0 & -\hat{\pi}^\dagger\hat{\pi} \end{bmatrix} + \frac{1}{t_\perp}\begin{bmatrix} 0 & (\hat{\pi})^2 \\ (\hat{\pi}^\dagger)^2 & 0 \end{bmatrix} . \quad (28)$$

To keep things simple, we consider in what follows the case $V = 0$; latter we will discuss the case $V \neq 0$. In cylindrical coordinates, the Hamiltonian (28) is written as

$$H_{BL} = -\frac{v_F^2\hbar^2}{t_\perp}\begin{bmatrix} 0 & L_-^2 \\ L_+^2 & 0 \end{bmatrix} , \quad (29)$$

and the eigenstates (regular at the origin) can be written as

$$|\varphi_m\rangle = \frac{1}{\sqrt{2A}}\begin{bmatrix} J_m(kr)e^{i\theta m} \\ \mp J_{m+2}(kr)e^{i\theta(m+2)} \end{bmatrix} , \quad (30)$$

to which corresponds the eigenvalues $E = \pm v_F^2\hbar^2k^2/t_\perp$. From this latter result, follows the density of states per spin, $\rho(E) = t_\perp/(\pi\sqrt{3}t^2)$.

It is important to stress two differences between the Hamiltonians (2) and (29) regarding boundary conditions and the nature of the scattering states. To be concrete, let us assume that electron is subjected to a potential well of the form $V(r) = V_0\theta(R - r)$. In the case of the Dirac Hamiltonian, the boundary conditions at the $r = R$ imply the continuity of the two components of the spinors, whereas for the bilayer Hamiltonian we have to impose the continuity of both the components of the spinors and their first derivative. The second aspect is related to the fact that elastic scattering conserves the energy. Then, since in bilayer graphene we have $E = \pm v_F^2\hbar^2k^2/t_\perp$, and keeping the energy constant, say $E > 0$, as in any scattering process, there are two admissible solutions for the values of k: a real value, $k = \sqrt{Et_\perp/(v_F^2\hbar^2)}$, and a pure imaginary one, $k = i\sqrt{Et_\perp/(v_F^2\hbar^2)}$. Therefore, bilayer graphene supports evanescent modes at the interface $r = R$. This fact is essential to satisfy the boundary conditions obeyed by the wave function.[?]

As in the case of the Dirac Hamiltoninan, we have to derive the form of the probability density current for electrons described by the Hamiltonian (29). The usual procedure[?] gives that any component, J_ℓ, of the current has the form

$$J_\ell = 2\frac{v_F^2\hbar}{t_\perp}\Im\langle\psi|\hat{J}_\ell|\psi\rangle , \quad (31)$$

where for $\ell = x, y$ we have

$$\hat{J}_x = \begin{bmatrix} 0 & \partial_x - i\partial_y \\ \partial_x + i\partial_y & 0 \end{bmatrix} , \quad (32)$$

and

$$\hat{J}_y = \begin{bmatrix} 0 & -i\partial_x - \partial_y \\ i\partial_x - \partial_y & 0 \end{bmatrix} . \quad (33)$$

For the radial component, $\ell = r$, we have

$$\hat{J}_r = \begin{bmatrix} 0 & e^{-2i\theta}(\partial_r + ir^{-1}\partial_\theta) \\ e^{2i\theta}(\partial_r - ir^{-1}\partial_\theta) & 0 \end{bmatrix} , \quad (34)$$

and for the tangential component, $\ell = \theta$, we have

$$\hat{J}_\theta = \begin{bmatrix} 0 & -ie^{-2i\theta}(\partial_r - ir^{-1}\partial_\theta) \\ ie^{2i\theta}(\partial_r + ir^{-1}\partial_\theta) & 0 \end{bmatrix} , \quad (35)$$

Taking into account that the Hamiltonian (29) forms a set of two coupled second-order differential equations, we assume that the asymptotic (large r) behavior of the wave function in the angular momentum channel m has the form

$$|\psi_m\rangle \simeq \frac{1}{\sqrt{2A}}\sqrt{\frac{2}{\pi kr}}\begin{bmatrix} \cos(kr - \lambda_m + \delta_m) \\ e^{2i\theta}\cos(kr - \lambda_m + \delta_m) \end{bmatrix} e^{i\delta_m} . \quad (36)$$

Following the same procedure we used to derive Eq. (16), we can show that the large-r behaviour of the total electronic wave function in graphene bilayer, in the presence of a potential, has the form

$$|\psi\rangle \simeq \frac{1}{\sqrt{2A}}\begin{pmatrix}1\\1\end{pmatrix}e^{ik_i x}+\frac{1}{\sqrt{2A}}\begin{pmatrix}1\\e^{2i\theta}\end{pmatrix}f(\theta)\frac{e^{ik_f r}}{\sqrt{r}}\,. \quad (37)$$

Using Eq. (31), we can show that the first term in Eq. (37) corresponds to a flux $J_x = 2v_F^2\hbar k/(At_\perp) \equiv v/A$, where v is the velocity of the particte, and that the second term corresponds to a radial flux of the form $J_r = 2v_F^2\hbar k|f(\theta)|^2/(rAt_\perp) \equiv v|f(\theta)|^2/(Ar)$, with $f(\theta)$ still given by Eq. (17). As before, it follows that the diferential cross section is given by Eq. (18).

In the following section, we will apply the introduced formalism to the case of a potential well described by the potential $V(r) = V_0\theta(R-r)$, in the strong interacting regime $V_0 \gg t$.

III. THE DC CONDUCTIVITY OF GRAPHENE AND ITS BILAYER

As we discussed in the introduction, there is a growing bulk of evidence that the limiting scattering mechanism of the electronic mobility in graphene can be described by strong short-range potentials, likely to be originated from adsorbed hydrocarbons. These adsorbed atoms and/or molecules act as resonant scatterers, giving rise to mid-gap states.[?]

A. Adsorbed atoms in graphene as strong short-range scattering centers

The resonant scattering mechanism is easy to seize by considering a simple toy model. Let us write the tight-binding Hamiltonian of the $\pi-$electrons in graphene as (spin index omitted)

$$H = -t\sum_{n,\boldsymbol{\delta}_i}|A,\boldsymbol{R}_n\rangle\langle\boldsymbol{R}_n+\boldsymbol{\delta}_i,B| + \text{H. c.}\,, \quad (38)$$

where $|\boldsymbol{A},\boldsymbol{R}_n\rangle$ represents the Wannier state at the unit cell $\boldsymbol{R}_n$, and the equivalent definition holds for $|B,\boldsymbol{R}_n+\boldsymbol{\delta}_i\rangle$, $\boldsymbol{\delta}_i$ is one of three nearest neighbor vectors in the honeycomb lattice, as depicted in Fig. 1.

We now consider that an impurity is binding covalently to a carbon atom at site $\boldsymbol{R}_n = 0$. Such a situation adds to the Hamiltonian (38) a term of the form

$$H_{\rm rs} = (V_{\rm ad}|\text{ad}\rangle\langle A,0| + \text{H. c.}) + \epsilon_{\rm ad}|\text{ad}\rangle\langle\text{ad}|\,, \quad (39)$$

where $V_{\rm ad}$ is the hybridization between the adatom (or a carbon atom of a hydrocarbon molecule) and a given carbon atom of graphene, $\epsilon_{\rm ad}$ is the relative (to graphene's carbon atoms) on-site energy of the electron in the adatom, and $|\text{ad}\rangle$ is the ket representing the state of the electron in the adatom. Taking the wave function to be of the form

$$|\psi\rangle = \sum_n[A(\boldsymbol{R}_n)|A,\boldsymbol{R}_n\rangle + B(\boldsymbol{R}_n+\boldsymbol{\delta}_2)|B,\boldsymbol{R}_n+\boldsymbol{\delta}_2\rangle] + C_{\rm ad}|\text{ad}\rangle\,, \quad (40)$$

the Schrödinger equation at the site $\boldsymbol{R}_n = 0$ reads

$$EA(0) - V_{\rm ad}C_{\rm ad} = -t[B(\boldsymbol{\delta}_1)+B(\boldsymbol{\delta}_2)+B(\boldsymbol{\delta}_3)]\,, \quad (41)$$

$$(E-\epsilon_{\rm ad})C_{\rm ad} = V_{\rm ad}A(0)\,. \quad (42)$$

Solving for $C_{\rm ad}$, we obtain

$$-t[B(\boldsymbol{\delta}_1)+B(\boldsymbol{\delta}_2)+B(\boldsymbol{\delta}_3)] = EA(0) - \frac{V_{\rm ad}^2A(0)}{E-\epsilon_{\rm ad}}\,. \quad (43)$$

The resonant effect is included in the last term of Eq. (43), which represents an effective local potential of the strength

$$V_{\rm eff} = V_{\rm ad}^2/(E-\epsilon_{\rm ad})\,. \quad (44)$$

It is the job of quantum chemical calculations to determine the value of the parameters $\epsilon_{\rm ad}$ and $V_{\rm ad}$.[???] The recently obtained typical values are $V_{\rm ad} \sim 2t \sim 5$ eV and $\epsilon_{\rm ad} \sim$ -0.2 eV,[?] leading to $V_{\rm eff} \sim 100$ eV, a rather strong on-site potential. Finally, the calculation of the transport properties, for such a model, can be performed using the $T-$matrix approach.[???] Its derivation for resonant scatterers is elementary, using the simple toy model described above. It is well known that the $T-$matrix for a local potential, of intensity v_0, reads[?]

$$T(E) = v_0[1-v_0\bar{G}_R(E)]^{-1}\,. \quad (45)$$

Then, using Eq. (44), the $T-$matrix due to an adatom must be of the form

$$T(E) = \frac{V_{\rm eff}}{1-V_{\rm eff}\bar{G}_R(E)} = \frac{V_{\rm ad}^2}{E-\epsilon_{\rm ad}-V_{\rm ad}^2\bar{G}_R(E)}\,. \quad (46)$$

Since we are considering that $V_{\rm ad} \gg (\epsilon_{\rm ad}, |E|)$, we can approximate the $T-$matrix (46) by

$$T(E) \approx -\frac{1}{\bar{G}_R(E)}\,, \quad (47)$$

which is nothing but the $T-$matrix for vacancies.[?]

Using Eq. (46), it simple to compute the transport relaxation time (at the Fermi surface), $\tau(k_F)$, using $\hbar/\tau(k_F) = \pi n_i^c|T(\epsilon_F)|^2\rho(\epsilon_F)$, where n_i^c is the concentration of impurities per unit cell, and k_F and ϵ_F are the Fermi momentum and energy, respectively. From the knowledge of $\tau(k_F)$, the conductivity of graphene follows from Boltzmann's transport equation.[?] For graphene, the function $\bar{G}_R(E)$ reads[?]

$$\bar{G}_R(E) = ED^{-2}\ln(E^2/D^2) - i\pi|E|/D^2\,, \quad (48)$$

with $D \simeq 3t$.

The above analysis made transparent that the effect of resonant scatterers is equivalent to that of a strong on-site potential. We can, then, use the formalism of the preceding section to compute the exact phase-shifts in the present of such a strong potential, from which $\tau(k_F)$ can also be obtained. Such type of calculations are equivalent, and alternative, to calculations based on the $T-$matrix approach.

The relation between $\tau(k_F)$ and $\sigma(\theta)$ is[?]

$$1/\tau(k_F) = n_i V_F \sigma_T\,, \quad (49)$$

where n_i is the concentration of impurities per unit area, V_F is the velocity of the electrons at the Fermi surface, and σ_T is the total transport cross section[?]

$$\sigma_T = \int_0^{2\pi} d\,\theta\sigma(\theta)(1-\cos\theta)\,, \\ = \frac{2}{k}\sum_{m=-\infty}^{\infty}\sin^2(\delta_m-\delta_{m+1}) \equiv \frac{2}{k}\Lambda(k)\,. \quad (50)$$

The conductivity of a given material follows from Boltzmann's transport equation. The electric current has the general form

$$\boldsymbol{j} = -\frac{g_s g_v e^2}{(2\pi)^2}\int d\,\boldsymbol{k}\tau(k)\frac{\partial n_F(k)}{\partial\varepsilon_k}\boldsymbol{v}\boldsymbol{v}\cdot\boldsymbol{E}\,, \quad (51)$$

where $n_F(x)$ is the Fermi distribution function, ε_k the dispersion of the electron, $\boldsymbol{v}$ the velocity of the particle, $\boldsymbol{E}$ the external electric field, and g_s and g_v the spin and valley degeneracies, respectively. The velocity, at the Fermi surface, of electrons in graphene read

$$\boldsymbol{V}_F = v_F(\cos\theta,\sin\theta)\,, \quad (52)$$

whereas in the bilayer it has the form

$$\boldsymbol{V}_F = \frac{2v_F^2}{t_\perp}\hbar k_F(\cos\theta,\sin\theta)\,, \quad (53)$$

which depends on the position of the Fermi energy; the quantity $M^{-1} = 2v_F^2/t_\perp$ plays the role of the electron's band mass. The DC conductivity, σ_{DC}, can be obtaining from writing Ohm's law as $j_x = \sigma_{DC}E_x$. Combining Eqs. (50), (51), (52), and (53), the conductivity σ_{DC}, for both monolayer and bilayer graphene, has one and the same form, namely

$$\sigma_{DC} = \frac{4e^2}{h}\frac{k_F^2}{4n_i\Lambda(k_F)}\,, \quad (54)$$

where the zero temperature limit has been taken. The importance of Eq. (54) could not be more emphasized, since it shows that the final dependence of the conductivity in k_F, and therefore in the electronic density, is controlled by the behavior of $\Lambda(k_F)$, which depends only on the phase-shifts δ_m; these, in turn, depend on the nature of the scattering potential. Therefore, the exact calculation of the phase-shifts emerge as the central theoretical problem regarding the description of σ_{DC} on the gate voltage for monolayer and bilayer graphene.

B. Graphene

For graphene and graphene bilayer, the electronic doping is controlled by a back-gate voltage V_g. The value of the Fermi momentum depends on the density of electrons, and, therefore, also on V_g. If the dielectric between graphene (or its bilayer) and the back-gate is made of silicon oxide and has a width of about 300 nm, then we have

$$k_F^2 = \pi\alpha V_g\,, \quad (55)$$

with $\alpha \simeq 7.2\times10^{10}$ V$^{-1}\cdot$cm^{-2}; numerically we have $k_F = 4.7\times10^{-3}\times\sqrt{V_g}$ Å^{-1}.

As we have discussed in Sec. III A, an adsorbed atom or molecule (of specific types) can be described as an effective strong short-range potential. As a consequence, we model the effect of an adsorbed chemical specie at the surface of graphene by a potential of the form

$$V(r) = V_0\theta(R-r)\,, \quad (56)$$

where R has to be of the order of $\sim$1Å and $V_0 \gg t$. As a limiting behavior, we shall consider that V_0 is made arbitrarily large.

In the limit $V_0\to\infty$, the potential defines an impenetrable barrier to the electronic probability flux. For electrons described either by the Schrödinger equation or by the Hamiltonian (29), the condiction of zero flux for $r\le R$ is achieved by imposing the condiction that $\psi(r=R)=0$ ($\psi(r)$ represents either a scalar or a spinor). For electrons described by the massless Dirac equation, this latter condiction implies that the wave function has to vanish everywhere, and, therefore, cannot be used. On the other hand, from Eq. (8) it is clear that the radial flux at $r=R$ can be made zero if one of the components of the spinor is zero at $r=R$.[?] In conclusion, the correct boundary condiction enforcing zero flux at $r=R$ is, for electrons in graphene, given by

$$\psi_i(r=R)=0\,, \quad (57)$$

where ψ_i, with $i=1,2$, is one of the components of the spinor. Given the presence of two Dirac cones in graphene, it is immaterial which component we may choose to obey condiction (57).

In order to satisfy the boundary condiction (57), we write the wave function describing the electrons being scattered by the barrier as

$$|\psi_m\rangle = A_1^m\begin{pmatrix} J_m(kr)\\ e^{i\theta}J_{m+1}(kr)\end{pmatrix} + A_2^m\begin{pmatrix} Y_m(kr)\\ e^{i\theta}Y_{m+1}(kr)\end{pmatrix}, \quad (58)$$

and the boundary condiction (57) implies that

$$\frac{A_2^m}{A_1^m} = -\frac{J_m(kR)}{Y_m(kR)}\,. \quad (59)$$

Since for large r, the wave function (58) must have the general form (11), it follows that the ratio A_2^m/A_1^m has to be interpreted as

$$\frac{A_2^m}{A_1^m} = -\tan\delta_m\,. \quad (60)$$

This latter equation defines the phase-shift δ_m. For back-gate values in the range $V_g \lesssim 100$ V, and considering $R\sim1$Å, we have $Rk<1$ (known as the low-energy scattering regime). In this regime, the scattering is dominated by the $s-$wave phase shift, that is, the dominant contribution to $\Lambda(k)$ comes from

$$\tan\delta_0 = \frac{J_0(kR)}{Y_0(kR)} \approx \frac{\pi}{2}\ln^{-1}(kR)\,, \quad (61)$$

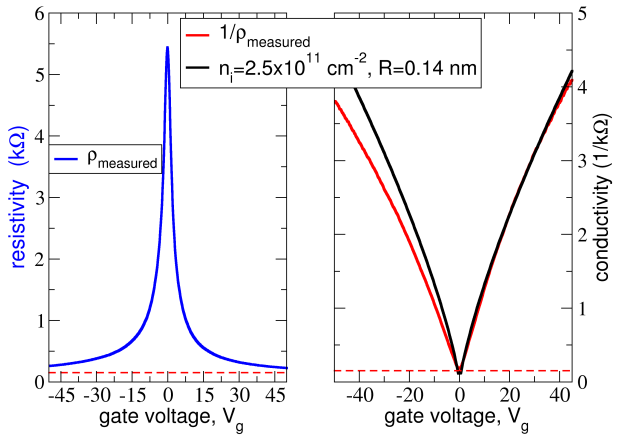

FIG. 3. (color online) **Left panel:** raw data of a measurement of the resistivity, $\rho_{\rm measured}$, of an exfoliated graphene sheet. **Right panel:** fit of the conductivity, $\sigma_{\rm sub} = 1/\rho_{\rm measured}$, using Eq. (62). The value of R was taken to be of the order of a_0 and the fit provided a concentration of impurities of $n_i \approx 2.5 \times 10^{11}$ cm^{-2}. (Data from S. V. Morozov *at al.*[?] , courtesy of A. K. Geim.)

where Eqs. (20) and (21) have been used. It follows from Eqs. (50) and (61) that the conductivity of graphene obtained from Eq. (54) has the final form[? ? ? ? ?]

$$\sigma_{DC} = \frac{4e^2}{h}\frac{k_F^2}{2\pi^2 n_i}\ln^2(k_F R)\,. \qquad (62)$$

Given that the value of R is constraint to be of the order of 1Å , n_i is the only fitting parameter. Eq. (62) was used to fit the conductivity data[?] of an exfoliated graphene sheet, as shown in Fig. 3. Because we took the limit $V_0 \to \infty$, the computed conductivity does not break electron-hole symmetry. The electron-hole asymmetry seen in the data of Fig. 3 can be both attributed to the presence of charge scatterers and/or to the role of the contacts.[?] If we increase the value of R some what, the concentrations of impurities needed to fit the data decreases. In Fig. 3 we have chosen to fit the conductivity for positive gate voltage; it is manifest that Eq. (62) fits accurately the data (solid red curve). If we had decided to fit the data for negative values of V_g, the obtained concentration of impurities, n_i, would habe been slightly different.

The result given by Eq. (62) for the conductivity of monolayer graphene, can also be obtained from a model where vacancies act as scattering centers.[?] In view of the arguments given in Sec. III A, such result comes with no surprise, since the effective local potential created by adsorbed hydrocarbons is much larger than the hopping integral t. Numerical simulations of the DC conductivity of graphene, based on Kubo's formula, under the effect of local potentials,[?] found a sublinear behavior for the DC conductivity of a graphene monolayer, in qualitative agreement with Eq. (62).

Let us now extend the previous analysis to the case of graphene bilayer.

C. Graphene bilayer

Assuming that the dominant source of scattering in graphene is due to strong short-range potentials, then the same must be true for bilayer graphene. As a consequence, a consistent description of electronic scattering in both monolayer and bilayer graphene must use same scattering potential to explain the measured conductivity in both systems. In the spirit of this work, this means that the scattering potential (56) must also be used to compute the conductivity of graphene bilayer.

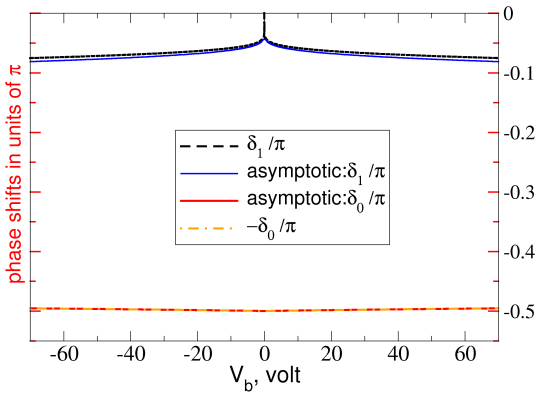

FIG. 4. (color online) Dependence of the exact and asymptotic phase-shifts δ_0 and δ_1 on V_g, for bilayer graphene.

As in the case of Eq. (58), we seek the form of the wave function as a superposition of Bessel functions of different kinds, which in the present case assumes the form

$$|\psi_m\rangle = A_1^m \begin{pmatrix} J_m(kr) \\ -e^{2i\theta}J_{m+2}(kr)\end{pmatrix} + A_2^m \begin{pmatrix} Y_m(kr) \\ -e^{2i\theta}Y_{m+2}(kr)\end{pmatrix} + A_3^m \begin{pmatrix} K_m(kr) \\ -e^{2i\theta}K_{m+2}(kr)\end{pmatrix}. \qquad (63)$$

The introduction of the modified Bessel function $K_m(kr)$ in Eq. (63) is necessary to satisfity the boundary condiction $\psi(r = R) = 0$. We recall that Hamiltonian (29) supports evanescent waves at the boundary $r = R$, as we discussed in Sec. II B. Futher, for large r, $K_m(kr)$ decays exponentially, as we can see from Eq. (19), and therefore, at large distances, the behavior of the wave function (63) depends only on the form of $J_m(kr)$ and $Y_m(kr)$, as given by Eqs. (12) and (13). As a consequence, the phase-shift δ_m is determined by the ratio A_2^m/A_1^m, that is, we must have

$$\frac{A_2^m}{A_1^m} = -\tan\delta_m\,, \qquad (64)$$

as in the case of electrons in monolayer graphene [see Eq. (60)]. Imposing the boundary condition $\psi(r = R) = 0$ on the wave function (63) we obtain

$$0 = A_1^m J_m(kR) + A_2^m Y_m(kR) + A_3^m K_m(kR)\,, \qquad (65)$$
$$0 = A_1^m J_{m+2}(kR) + A_2^m Y_{m+2}(kR) + A_3^m K_{m+2}(kR)\,. \qquad (66)$$

from which follows

$$\frac{A_2^m}{A_1^m} = \frac{J_m(kR)K_{m+2}(kR) - J_{m+2}(kR)K_m(kR)}{K_m(kR)Y_{m+2}(kR) - K_{m+2}(kR)Y_m(kR)} . \quad (67)$$

Combining Eqs. (64) and (67) the equation for the phase-shift δ_m follows at once. As in the case of monolayer graphene, the cross section is dominated by δ_0. The asymptotic expansions for δ_0 and δ_1 are ($k_F R < 1$)

$$\tan\delta_0 = -\frac{2}{\pi}(k_F R)^{-2}[\ln(k_F R/2) + \gamma_E]^{-1} \Rightarrow \delta_0 \approx \frac{\pi}{2} , \quad (68)$$

and

$$\tan\delta_1 = \frac{\pi}{4}[\ln(k_F R/2) + \gamma_E]^{-1} \Rightarrow \delta_1 \approx \tan\delta_1 , \quad (69)$$

where $\gamma_E = 0.577\ldots$ is Euler's constant. The dependence of δ_0 and δ_1 on V_g is given in Fig. 4. From δ_0 and δ_1, it follows

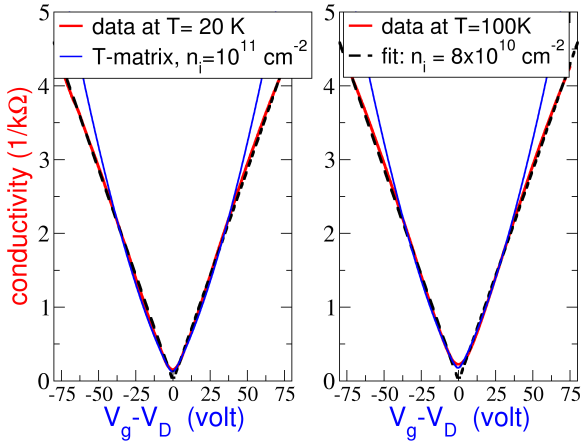

FIG. 5. (color online) Fit of the conductivity data of bilayer graphene (solid red curve) using Eq. (70) and Eq. (73). The fit has only a single parameter, the concentration of impurities. The obtained value is $n_i \approx 8\times10^{10}$ cm^{-2}, for Eq. (70), and $n_i \approx 1\times10^{11}$ cm^{-2} for the $T-$matrix approach, using a model of pure vacancies, Eq. (73). The **left panel** shows data taken at a temperature of 20 K, whereas the **right panel** shows the conductivity of the same sample at the higher temperature of 100 K. The position of the Dirac point, V_D, was shifted to zero in this figure. (Data from S. V. Morozov *at al.*[?], courtesy of A. K. Geim.)

that $\Lambda(k_F) \approx 2$. The DC conductivity of bilayer graphene is, therefore, given by

$$\sigma_{DC} = \frac{4e^2}{h}\frac{k_F^2}{8n_i} . \quad (70)$$

We have used Eq. (70) to fit the conductivity data of an exfoliated bilayer graphene sample, as shown in Fig. 5. The fit provides a concentration of impurities of the order of $n_i \approx 8\times10^{10}$ cm^{-2}.

Within the $T-$matrix approach, the DC conductivity of bilayer graphene has been computed in the past.[? ?] The impurity concentrations used in those works were far too large to make apparent the linear behavior in V_g given by Eq. (70). We have already shown that the effect of resonant scatterers can be captured by a model of pure vacancies, both using the $T-$matrix and the partial wave approaches. We now revisit the $T-$matrix calculation in bilayer graphene[? ? ?] and show that, as in the case of the monolayer, a model of pure vacancies in bilayer also capture the physics of resonant scatterers.

D. $T-$matrix approach for graphene bilayer

In Refs. **? ?** the calculation of the DC conductivity took into account the full band structure of the graphene bilayer. That calculation could distinguish between the four carbon atoms in the unit cell. In this section we assume that vacancies are located at the two carbon that are not coupled by $t_\perp$.

In the notation of Refs. **? ?** , the DC conductivity (at $T = 0$) obtained from the Kubo formula is

$$\sigma_{DC} = \frac{8e^2}{\pi h}\int_0^{\Lambda^2} d(k^2)\left\{\Im[g^D_{AA}(E_F,k)]\Im[g^D_{BB}(E_F+\delta,k)] + \Im[g^{ND}_{AB}(E_F,k)]\Im[g^{ND}_{AB}(E_F+\delta,k)]\right\} , \quad (71)$$

in the limit $\delta \to 0$. The k^2-integral can be performed exactly as explained in Appendix C of Ref. **?** . The resulting complicated formula can be approximated by going through the following steps: (i) neglect the real part of the self-energies, (ii) expand the result in powers of the imaginary part of the self-energies $\Gamma_a(\epsilon) \equiv -\mathrm{Im}[\Sigma_a(\epsilon)]$, and (iii) assume that the energies involved fulfill $|\mu|, t_\perp \pm |\mu| \gg \Gamma_A(\epsilon), \Gamma_B(\epsilon)$. The leading term in this expansion leads to the approximate formula

$$\sigma_{DC} \approx \frac{2e^2}{h}\frac{E_F(E_F+t_\perp)}{t_\perp\Gamma_B(E_F) + E_F[\Gamma_A(E_F)+\Gamma_B(E_F)]} . \quad (72)$$

This expression is a good approximation for small impurity concentrations and away from the neutrality point, at which the condition in (iii) breaks down. This result may be further simplified using the relation between the Fermi energy and the density (assuming $n, E_F > 0$) coming from the dispersion relation $E_F = \sqrt{(t_\perp/2)^2 + \pi(\hbar v_F)^2 n} - t_\perp/2$, to

$$\sigma_{DC} = \frac{2e^2}{h}\frac{\pi(\hbar v_F)^2 n}{t_\perp\Gamma_B(E_F) + E_F[\Gamma_A(E_F)+\Gamma_B(E_F)]} , \quad (73)$$

where n is the electronic density. To the extent that the denominator is independent of E_F, the conductivity is then linear in the density of carriers, n, in agreement with the description based on the phase-shifts. Equation (73) was derived using the T-matrix, which is written in terms of the bare Green's functions. For low impurity density, as is the case in exfoliated samples, the difference between the conductivity obtained from the CPA and the T-matrix is very small except in a tiny region near the neutrality point. The data in Fig. (5) can be reasonably fit considering a density of vacancies of $n_i \simeq 10^{11}$ cm^{-2}.

IV. SCATTERING IN A BIASED BILAYER GRAPHENE

When $V \neq 0$, electrons in a graphene bilayer are described by Eq. (28). In this case, the energy spectrum develops a Mexican hat form, has represented in Fig. 6. When the energy of the electrons is smaller than V, the Fermi surface becomes a ring around the Dirac point, with an inner, k_-, and an outer, k_+, Fermi radii in momentum space. Therefore, for $E < V$, we have two degenerate states with different momentum values. As we will show below, the description of scattering in these to regimes, $E \gtrless V$, are necessarily different.

The regular eigenstates of Hamiltonian (28) in polar coordinates are given by

$$|\varphi_m\rangle = \frac{1}{\sqrt{A}} \begin{bmatrix} a_k J_m(kr) e^{i\theta m} \\ \mp b_k J_{m+2}(kr) e^{i\theta(m+2)} \end{bmatrix}, \tag{74}$$

to which corresponds the eigenvalues

$$E(k) = \pm\sqrt{V^2(1-\epsilon_k/t_\perp)^2 + \epsilon_k^2}\,, \tag{75}$$

where $\epsilon_k = v_F^2\hbar^2k^2/t_\perp$ is the energy of electrons in bilayer graphene for $V = 0$, and the coefficients a_k and b_k read

$$a_k = \sqrt{\frac{1}{2}}[1 + V(1-\epsilon_k/t_\perp)/E]^{1/2}\,, \tag{76}$$

$$b_k = \sqrt{\frac{1}{2}}[1 - V(1-\epsilon_k/t_\perp)/E]^{1/2}\,. \tag{77}$$

Additionally, we have the relation $a_k^2 b_k^2 = \epsilon_k^2/(4E^2)$. The

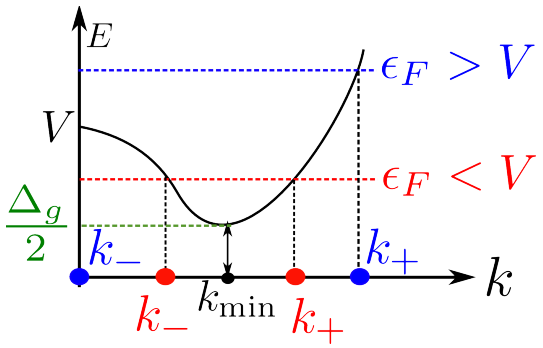

FIG. 6. (color online) Energy spectrum of a biased graphene bilayer. The figure depicts several quantities defined in the text, and ϵ_F stands for the Fermi energy. The figure contains information on the two regimes $E \gtrless V$.

density probability flux, J_ℓ, is given, for $\ell = x, r$, by Eq. (31) plus the additional term J_ℓ^V reading

$$J_\ell^V = 2V\frac{v_F^2\hbar}{t_\perp^2}\Im\langle\psi|\hat{J}_\ell^V|\psi\rangle\,, \tag{78}$$

where, for $\ell = x, r$, the operator $\hat{J}_\ell^V$ is given by

$$\hat{J}_\ell^V = \begin{bmatrix} -\partial_\ell & 0 \\ 0 & \partial_\ell \end{bmatrix}. \tag{79}$$

Let us establish here some useful relations for latter use. The energy gap, Δ_g, is determined from

$$\Delta_g = 2E(k_{\rm min}) = 2Vt_\perp[V^2 + t_\perp^2]^{-1/2}\,, \tag{80}$$

where $k_{\rm min}$ is defined in Eq. (82). Given a state with energy E, the two momentum values are obtained from the inversion of the energy spectrum (75), and are given by the positive roots of the following equation

$$\frac{\epsilon_k}{t_\perp} = \frac{\Delta_g^2}{4t_\perp^2}\left[1 \pm \sqrt{1-(1+t_\perp^2/V^2)(1-E^2/V^2)}\right]. \tag{81}$$

From Eq. (81) we see that for $E < V$ the two roots are real, corresponding to two propagating states, whereas for $E > V$ only one root is real, corresponding to a single propagating state; this is consistent with the dispersion depicted in Fig. 6. In this latter regime, the imaginary root is, nevertheless, essential to fulfill the scattering boundary conditions, as in the case discussed in Sec. II B. For the energy $E = V$, we are at the boundary between the two regimes introduced above, $E \gtrless V$. In this case, the scattering descriptions below and above $E = V$ must provide the same answer. For $E = V$ we have $k_- = 0$ and $k_+ = \Delta_g/(\sqrt{2}v_F\hbar) = \sqrt{2}k_{\rm min}$; for $E < V$ we have a simple relation between k_- and k_+ reading

$$k_- = \sqrt{2k_{\rm min}^2 - k_+^2}\,, \quad k_{\rm min} = \frac{\Delta_g}{2v_F\hbar}\,. \tag{82}$$

The velocity of the electrons at k_- and k_+ is given by

$$v_r(k) = \frac{\partial E(k)}{\hbar\partial k} = \pm\frac{2v_F^2\hbar k}{t_\perp}\frac{V^2}{t_\perp E} \times \\ \times\sqrt{1-(1+t_\perp^2/V^2)(1-E^2/V^2)}\,. \tag{83}$$

Clearly, the state with momentum k_- has negative velocity; the scattering formalism has to take this aspect into account.

Because the regimes $E > 0$ and $E < 0$ are distinct, in the sense that the latter case contains two degenerate propagating states, we will develop the scattering theory separately for both cases.

A. The $E > V$ regime

For $E > V$, the two momenta are $k_+ = k$ and $k_- = i\sqrt{k_+^2 - 2k_{\rm min}^2} = i\kappa$. This latter value originates an evanescent wave at the boundary of the potential. As in the case of Sec. II B, it is simple to show that a wave function of the form

$$|\psi\rangle \simeq \frac{1}{\sqrt{A}}\begin{pmatrix} a_{k_x} \\ b_{k_x} \end{pmatrix} e^{ik_i x} + \frac{1}{\sqrt{A}}\begin{pmatrix} a_k \\ b_k e^{2i\theta} \end{pmatrix} f(\theta)\frac{e^{ik_f r}}{\sqrt{r}}\,, \tag{84}$$

represents an incoming plane wave of momentum $\boldsymbol{k}_i = (k_+, 0) = (k, 0)$ and a scattered cylindrical wave of momentum $\boldsymbol{k}_f = k_+(\cos\theta, \sin\theta)$. The scattered radial flux has the usual form $J_r = v_r|f(\theta)|^2/r$, from which the differential

cross section follows as $\sigma(\theta) = |f(\theta)|^2$. As in the case of Sec. III C, we seek the form of the wave function as a superposition of Bessel functions of different kinds, which in the present case assumes the form

$$|\psi_m\rangle = A_1^m \begin{pmatrix} a_k J_m(kr) \\ -b_k e^{2i\theta} J_{m+2}(kr) \end{pmatrix} + A_2^m \begin{pmatrix} a_k Y_m(kr) \\ -b_k e^{2i\theta} Y_{m+2}(kr) \end{pmatrix} + A_3^m \begin{pmatrix} a_\kappa K_m(\kappa r) \\ -b_\kappa e^{2i\theta} K_{m+2}(\kappa r) \end{pmatrix} . \quad (85)$$

The ratio A_m^2/A_1^m reads

$$\frac{A_2^m}{A_1^m} = \frac{a_k b_\kappa J_m(kR)K_{m+2}(\kappa R) - b_k a_\kappa J_{m+2}(kR)K_m(\kappa R)}{b_k a_\kappa K_m(\kappa R)Y_{m+2}(kR) - a_k b_\kappa K_{m+2}(\kappa R)Y_m(kR)} , \quad (86)$$

Combining Eqs. (64) and (86) the equation for the phase-shift δ_m follows at once. In the regime $k_+ \gg \sqrt{2}k_{\min}$ we have $\kappa \approx k_+ = k$, $a_k \approx a_\kappa$, and $b_k \approx b_\kappa$, and therefore the phase-shifts given by Eq. (67) and (86) are essentially identical, that is, we have

$$\delta_0 \to \frac{\pi}{2} , \quad (k_+ \gg \sqrt{2}k_{\min}) , . \quad (87)$$

As a consequence of (87), the conductivity is linear in V_g, at high electronic density.

When the gate voltage is reduced bringing (from above) the Fermi energy close to V, we have $\kappa \to 0$, but $k_+ \gtrsim \sqrt{2}k_{\min}$ finite. In this case we have

$$\frac{A_2^m}{A_1^m} \to -\frac{J_m(kR)}{Y_m(kR)} , \quad (88)$$

and considering that $kR \lesssim 1$, the $s-$wave phase shift tends to

$$\delta_0 \to \frac{\pi}{2} \ln^{-1}(kR) , \quad (k_+ \gtrsim \sqrt{2}k_{\min}) . \quad (89)$$

The dependence of the conductivity on k_F requires taking into account the dependence of the velocity in k_F.

B. The $E < V$ regime

As we discussed at the beginning of Sec. IV, for $E < V$ there are two degenerate propagating states, characterized by k_- and k_+. In this case, the matrix element of the potential between these two states is finite, and an incoming particle with a well defined momentum (k_- or k_+) will be scattered in a superposition of both momenta, as depicted in Fig. 7. This fact requires the modification of the scattering formalism introduced above. In the spirit of Fig. 7, we will develop the scattering formalism assuming that the incoming electron has momentum k_+; the case where the incoming electron has momentum k_- follows immediately and only the final results will be given.

We start by assuming that the total wave function in the presence of the potential, at large distances from it, has the

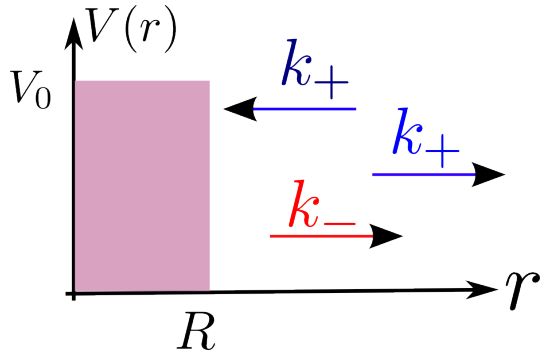

FIG. 7. (color online) Scattering by a potential of strength V_0 and range $r = R$ in the regime $E < 0$. In the figure, we represent the case where the incoming electron comes with momentum k_+ and is scattered in a superposition of two degenerate propagating waves, with momenta k_+ and k_-.

asymptotic form

$$|\psi\rangle \simeq \frac{1}{\sqrt{A}} \begin{pmatrix} a_{k_x} \\ b_{k_x} \end{pmatrix} e^{ik_+ x} + \frac{1}{\sqrt{A}} \begin{pmatrix} a_{k_+} \\ b_{k_+} e^{2i\theta} \end{pmatrix} f_{++}(\theta) \frac{e^{ik_+ r}}{\sqrt{r}} + \frac{1}{\sqrt{A}} \begin{pmatrix} a_{k_-} \\ b_{k_-} e^{2i\theta} \end{pmatrix} f_{+-}(\theta) \frac{e^{-ik_- r}}{\sqrt{r}} , \quad (90)$$

where $f_{++}(\theta)$ represents the scattering amplitude considering that the outgoing electron has the same momentum, k_+, as the incoming one, and $f_{+-}(\theta)$ represents the scattering amplitude considering that the outgoing electron changed its momentum to k_-. Let us stress again that $E(k_-) = E(k_+)$. Since the velocity of the state with momentum k_- is negative, the sign of the argument in the exponential of associated cylindrical wave function has to been negative, since these states represent particles propagating backwards in time (a positive sign gives a radial incoming flux). The flux associated with the first, second, and third terms on the righthand side of Eq. (90) read

$$J_x^+ = v_x(k_+) , \quad (91)$$
$$J_r^+ = v_r(k_+)|f_{++}(\theta)|^2 r^{-1} , \quad (92)$$
$$J_r^- = -v_r(k_-)|f_{+-}(\theta)|^2 r^{-1} , \quad (93)$$

respectively, from which follows the existance of two scattering cross sections, defined as

$$\sigma{+}{+}(\theta) = |f_{++}(\theta)|^2 , \quad \sigma{+}{-}(\theta) = -\frac{v_r(k_-)}{v_r(k_+)}|f_{+-}(\theta)|^2 . \quad (94)$$

Both these two cross sections must enter in the relaxation time needed to compute the DC conductivity.

We shall now assume that partial wave in the angular momentum basis of the total wave function has, at large distances from the potential, the form

$$|\psi_m\rangle \simeq \frac{1}{2\sqrt{A}} \begin{pmatrix} a_{k_+} \\ b_{k_+} e^{2i\theta} \end{pmatrix} e^{-i(k_+ r - \lambda_m)} + \frac{1}{2\sqrt{A}} \eta_{m,++} e^{2i\delta_{m,++}} \begin{pmatrix} a_{k_+} \\ b_{k_+} e^{2i\theta} \end{pmatrix} \frac{e^{i(k_+ r - \lambda_m)}}{\sqrt{r}} + \frac{1}{2\sqrt{A}} \eta_{m,+-} \begin{pmatrix} a_{k_-} \\ b_{k_-} e^{2i\theta} \end{pmatrix} \frac{e^{-i(k_- r - \lambda_m)}}{\sqrt{r}} , \quad (95)$$

where $\delta_{m,++}$ is the phase shift of the partial wave m and $0 < \eta_{m,++} < 1$ is real number accounting for the transfer of probability flux to the outgoing momentum channel k_-, and $0 < |\eta_{m,+-}|^2 < 1$. Conservation of the radial flux for each partial wave m imposes

$$\eta_{m,++}^2 + |\eta_{m,+-}|^2 = 1 . \quad (96)$$

Summing over m according to Eq. (11) we obtain $|\psi\rangle$ in the form given by Eq. (95), with the scattering amplitudes defined as

$$f_{++} = \frac{1}{\sqrt{2\pi k_+}} \sum_m (i)^m (\eta_{m,++} e^{2i\delta_{m,++}} - 1) e^{i(\theta m - \lambda_m)} , \quad (97)$$

$$f_{+-} = \frac{1}{\sqrt{2\pi k_-}} \sum_m (i)^m \eta_{m,+-} e^{i(\theta m - \lambda_m)} . \quad (98)$$

As in Sec. II B, we write the exact partial wave of the full scattering problem, for $r > R$, as

$$|\psi_m\rangle = A_1^m \begin{pmatrix} a_{k_+} H_m^{(2)}(k_+ r) \\ -b_{k_+} H_{m+2}^{(2)}(k_+ r) e^{2i\theta} \end{pmatrix} + A_2^m \begin{pmatrix} a_{k_+} H_m^{(1)}(k_+ r) \\ -b_{k_+} H_{m+2}^{(1)}(k_+ r) e^{2i\theta} \end{pmatrix} + A_3^m \begin{pmatrix} a_{k_-} H_m^{(2)}(k_- r) \\ -b_{k_-} H_{m+2}^{(2)}(k_- r) e^{2i\theta} \end{pmatrix} . \quad (99)$$

Expanding Eq. (99) for large r and comparing it with Eq. (95), we see that

$$\frac{A_2^m}{A_1^m} = \eta_{m,++} e^{2i\delta_{m,++}} , \quad \frac{A_3^m}{A_1^m} = \eta_{m,+-} . \quad (100)$$

The calculation of the diferential cross section requires the determination of $\eta_{m,++}$, $\eta_{m,+-}$, and $\delta_{m,++}$. In the limit $V_0 \to \infty$, the boundary condiction is $\psi_m(r = R) = 0$, leading to

$$\frac{A_2^m}{A_1^m} = \eta_{m,++} e^{2i\delta_{m,++}} = \frac{a_{k_+} b_{k_-} H_m^{(2)}(k_+ R) H_{m+2}^{(2)}(k_- R) - b_{k_+} a_{k_-} H_{m+2}^{(2)}(k_+ R) H_m^{(2)}(k_- R)}{b_{k_+} a_{k_-} H_m^{(2)}(k_- R) H_{m+2}^{(1)}(k_+ R) - a_{k_+} b_{k_-} H_{m+2}^{(2)}(k_- R) H_m^{(1)}(k_+ R)} , \quad (101)$$

$$\frac{A_3^m}{A_1^m} = \eta_{m,+-} = -a_{k_+} b_{k_+} \frac{H_{m+2}^{(1)}(k_+ R) H_m^{(2)}(k_+ R) - H_m^{(1)}(k_+ R) H_{m+2}^{(2)}(k_+ R)}{b_{k_+} a_{k_-} H_m^{(2)}(k_- R) H_{m+2}^{(1)}(k_+ R) - a_{k_+} b_{k_-} H_{m+2}^{(2)}(k_- R) H_m^{(1)}(k_+ R)} . \quad (102)$$

Although not immediately obvious (the reader can always check it numerically), the parameters $\eta_{m,++}$ and $\eta_{m,+-}$, as give by Eqs. (101) and (102), obey the flux conservation relation (96). When the Fermi energy, ϵ_F, approaches the energy $E = V$ from below, we have $k_- \to 0$. In this limit we find

$$\eta_{0,++} e^{2i\delta_{0,++}} \to -\frac{H_0^{(2)}(k_+ R)}{H_0^{(1)}(k_+ R)} , \quad (103)$$

$$\eta_{m,+-} \to 0 , \quad (104)$$

as it should. Since $k_+ R \lesssim 1$, it follows from Eq. (103) that

$$e^{2i\delta_{0,++}} \to \frac{2\ln(k_+ R) + i\pi}{2\ln(k_+ R) - i\pi} , \quad (105)$$

which gives for $\delta_{0,++}$ the same result found in Eq. (89).

C. DC conductivity of a biased bilayer graphene

As already discussed in Sec. III C, the calculation of the DC conductivity requires the computation of the exact phase-shifts. We start by studying the behaviour of the $s-$wave phase shift as function of the Fermi momentum for a biased graphene bilayer.

In the biased bilayer, the ability of tunning the electronic density and the value of the gap, Δ_g, independently requires the use of two gates: a bottom and a top gates, as shown in Fig. 8. The electric field in the top-gate dielectric is ($e > 0$)

$$E_t = \frac{e n_t}{\epsilon_t \epsilon_0} , \quad (106)$$

and in the bottom-gate dielectric is

$$E_b = \frac{e n_b}{\epsilon_b \epsilon_0} , \quad (107)$$

where n_t and n_b are the electronic density in the top and bottom gate, respectively, and ϵ_t and ϵ_b are the relative permittivity of the top and bottom gate dielectric, respectively. Charge neutrality requires that the total amount of charge accommulated in the bilayer is $-en = -e(n_t + n_b)$. The electrostatic potential difference between the top gate and the bilayer is $V_t = tE_t$, whereas between the bottom gate and the bilayer is

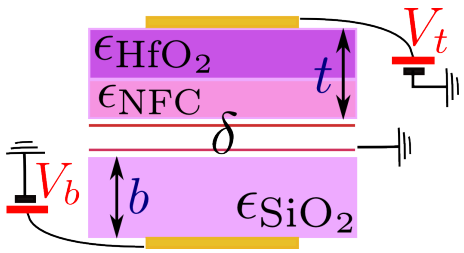

FIG. 8. (color online) Capacitor geometry for dual gate transistor.[?] The figure is self-explanatory. The values of the several quantities are: $\epsilon_{\mathrm{SiO_2}} = 3.9$, $\epsilon_{\mathrm{HfO_2}} = 25$, $\epsilon_{\mathrm{NFC}} = 2.4$, $b = 300$ nm, $t = 20$ nm. The quantities V_t and V_b stand for the top and bottom gate potentials, respectively.

$V_t = bE_b$. It follows from Eqs. (106) and (107) that

$$V_b = b\frac{en_b}{\epsilon_b\epsilon_0} = \frac{ben}{\epsilon_b\epsilon_0} - \frac{b\epsilon_t}{t\epsilon_b}V_t\,. \tag{108}$$

Inverting Eq. (108), the total electronic density in the bilayer is given by

$$n = V_g\frac{\epsilon_b\epsilon_0}{be} + \frac{\epsilon_0\epsilon_t}{et}V_t\,. \tag{109}$$

When n is positive, the bilayer is doped with electrons, if n is negative the system is doped with holes. Finally, the electrostatic potential difference between the two graphene layers in the bilayer is given by

$$\Delta V = (E_b - E_t)\delta = \frac{ne\delta}{\epsilon_b\epsilon_0} - \left(\frac{\epsilon_t}{\epsilon_b} + 1\right)\frac{\delta}{t}V_t\,, \tag{110}$$

where $\delta = 3.4$ Åis the inter-layer distance. The variable of V introduced in Eq. (26) relates to ΔV as $2V = \Delta V$. Taking typical values for dual gate bilayer-transistors,[?] we have: $\epsilon_{\mathrm{SiO_2}} = 3.9$, $\epsilon_{\mathrm{HfO_2}} = 25$, $\epsilon_{\mathrm{NFC}} = 2.4$, $b = 300$ nm, $t = 20$ nm (both dielectrics, HfO_2 and NFC, having about the same width). The relative permitivity of ϵ_t is

$$\epsilon_t = \frac{2\epsilon_{\mathrm{HfO_2}}\epsilon_{\mathrm{NFC}}}{\epsilon_{\mathrm{HfO_2}} + \epsilon_{\mathrm{NFC}}}\,. \tag{111}$$

In working devices,[?] we have $-70 \lesssim V_b \lesssim 70$ and $-4 \lesssim V_t \lesssim 4$.

The calculation of DC conductivity follows, as before, from Boltzmann's transport theory. In the regime $E > V$, σ_{DC} is still given by Eq. (54), but with the phase-shifts determined from (86).

When $E < V$, there are two scattering channels and this implies that resulting formula for σ_{DC} differs somewhat from that given in Eq. (54), reading

$$\sigma_{\mathrm{DC}} = \frac{4e^2}{h}\frac{1}{2}\left[\frac{k_+}{n_i\sigma(k_+)} + \frac{k_-}{n_i\sigma(k_-)}\right]\,, \tag{112}$$

where $\sigma(k_\pm)$ is defined has

$$\sigma(k_\pm) = \int_0^{2\pi}[\sigma_{\pm,+}(\theta) + \sigma_{\pm,-}(\theta)](1-\cos\theta)\,. \tag{113}$$